COUETTE FLUID FLOW THROUGH PARALLEL RIGA PLATE WITH ELECTROMAGNETIC FIELD

NASRIN, S.[1*] – MONDAL, R. N.[1] – ALAM, M. M.[2]

[1] *Department of Mathematics, Jagannath University, Dhaka, Bangladesh.*

[2] *Mathematics Discipline, Khulna University, Khulna, Bangladesh.*

**Corresponding author*
e-mail: sn_mri[at]yahoo.com

(Received 07th September 2023; accepted 10th December 2023)

Abstract. The steady-state solution of Couette fluid flow through a parallel Riga plate with an electromagnetic field has been investigated. The system "Riga plate" refers to a specially designed surface with a grid of alternating electrodes that interacts with an electric or magnetic field to affect the behavior of fluid flow. This type of system might induce electromagnetic forces or induce a magnetic field in the fluid, leading to changes in its flow pattern. It is mostly utilized in industrial operations involving fluid flow issues. This is an attempt to research the impacts of viscous dissipation effects, thermal radiation, and melting heat on the Riga plate. The Riga plate can be used to control fluid flow in situations where an external magnetic or electric field is necessary because it functions as a tool to lessen skin friction and improve the phenomenon of heat transfer. Increased heat transfer in industrial processes or heat exchangers may result in more effective fluid-to-fluid energy transfer, which may enhance system performance as a whole. Additionally, it reduces the impacts of turbulence effects, making it easy to manage flow effectively and enhancing machine performance. The mathematical model includes the system of governing momentum and energy equations. The primary approach to solving the problem has been the explicit finite difference method. Matlab R2015a has been used as a secondary tool to simulate the results. For a number of variables of the dimensionless parameter, including the pressure gradient parameter, modified Hartmann number, Prandtl number, and Eckert number, the estimated results have been obtained. In the presence of the Riga plate, Eckert number helps to increase temperature and the modified Hartmann number impacts convective heat transmission because they slow down the fluid's motion. It may be inferred that as the modified Hartmann number increases, the MHD fluid's heat transmission mode gradually shifts from convection to conduction. It is possible that a large enough modified Hartmann number may completely halt the fluid's movement. Then, only conduction would be used to transmit heat. Graphical representations have been employed to illustrate the impact of relevant parameters on different distributions. Additionally, the skin friction and Nusselt number expressions have been presented alongside these visuals.
Keywords: *couette flow, magnetic field, riga plate, explicit finite difference*

Introduction

Classical MHD flow control, influenced by an external magnetic field, is a method of controlling highly conductive fluids. Electro-magneto hydrodynamic (EMHD) flow is the term used to describe the flow that results when a fluid's electrical conductivity is too low, causing the Lorentz force to diminish exponentially. The Riga plate constitutes an electromagnetic surface crafted from permanent magnets and electrodes. Its design aims to furnish a planar surface devoid of distinct polarity and magnetization. This technology generates electromagnetic and hydrodynamic fluid flow. Additionally, it separates the boundary layer while simultaneously reducing the impact of turbulence, resulting in a better flow pattern. The inception of the Riga plate formulation dates back to 1961 and is recognized as the work of Gailitis (1961). It has several important uses, including biomechanics, chemical engineering, magneto-aerodynamics, civil

engineering, mechanical engineering etc. Soundalgekar et al. (1979) explored the impact of natural convection on the Stokes problem, specifically addressing a vertical plate exposed to a magnetic field applied transversely. Sacheti et al. (1994) obtained an exact solution for the unsteady magneto-hydrodynamic (MHD) free convection flow over a vertical plate undergoing a sudden onset with a consistent heat flux. Pantokratoras and Magyari (2009) proposed a model for electro-magneto-hydrodynamic free convection fluid flow characterized by low conductivity along a Riga plate. Following this, Pantokratoras (2011) investigated whether the Riga plate is stationary within a constant free stream or moves within such a flow. Ayub et al. (2016) examined the interaction between an electromagnetic actuator, commonly known as a Riga plate, and a nanofluid flow influenced by electromagnetic hydrodynamics (EMHD).

Ahmed et al. (1998) used a vertical Riga plate and intense suction to perform mixed convection of a nanofluid flow. The utilization of magnetohydrodynamic (MHD) laminar flow through porous media holds considerable significance, especially in engineering and agricultural processes, groundwater dynamics, the petroleum industry, and the purification of oil and gas. Al-Nimr and Masoud (1998) performed an examination of the unsteady free convection flow in a porous medium along a flat plate. Angirasa and Peterson (1997) conducted a numerical study on heat transfer in the natural convection process from an isothermal vertical surface, particularly through a stable layered fluid-saturated thermally stratified porous medium. Ravikumar et al. (2012) explored the discourse on three-dimensional Couette flow with heat transfer through a porous medium, confined by infinite vertical porous plates. Yabo et al. (2018) elucidated the destabilizing impact of a transverse magnetic field on the free-convective Couette flow of a conducting fluid, taking into account the influence of thermal radiation. Raptis and Kafousias (1982) investigated the repercussions of free convection on the flow characteristics of an incompressible, viscous fluid flowing through a vertically infinite porous plate undergoing acceleration in its plane. Hasimoto (1957) utilized an infinite flat plate with uniform suction and injection to examine boundary layer formation. Under conditions of uniform suction and injection, he derived an exact solution to the Navier-Stokes equations of motion. Fang (2004) further investigated the incompressible Couette flow with porous plates, obtaining an exact solution for the unsteady velocity. Das et al. (2009) investigated the influence of the magnetic field and rotation on the unsteady magneto-hydrodynamic (MHD) Couette flow between infinite horizontal parallel plates within a rotating system. Chauhan and Rastogi (2009) conducted a study examining the flow of a viscous, incompressible, electrically conducting fluid in a horizontally oriented parallel plate channel subject to rotation, with the added influence of an inclined magnetic field.

Attia and Ewis (2010) investigated the heat transfer dynamics in the unsteady magneto-hydromagnetic Couette flow of a non-Newtonian viscoelastic fluid, which is electrically conducting and incompressible, between two parallel porous horizontal plates that are non-conducting. Seth et al. (2011) characterized the movement of an incompressible, electrically conductive fluid with viscosity between two porous plates arranged in parallel, influenced by a transverse magnetic field. They termed this phenomenon an unsteady magneto-hydrodynamic (MHD) Couette flow. Beg et al. (2009) investigated the influence of Hall current and heat transfer in the realm of unsteady magneto-hydrodynamic Couette flow within a channel made of porous media. In their research, Ochoa-Tapia and Whitaker (1995a; 1995b) postulated stress jump circumstances at the fluid-porous interface when viscous fluid moves next to a porous

medium. In the investigation of Couette flow within a composite channel, where a portion is filled with a porous medium and another portion with a transparent fluid, and under similar jump conditions, Kuznetsov (1998) conducted a study. Muhuri (1963) investigates the evolution of Couette flow between two parallel walls at low magnetic Reynolds numbers. This flow originates from the sudden and uniformly accelerated motion of one wall in an electrically conducting, viscous, and incompressible fluid, with constant suction velocity applied to the walls. Based on the aforementioned expressions, a brief discussion on the investigation of Couette fluid flow through a parallel Riga plate with an electromagnetic field has been provided. The graphical presentation illustrates the behavior of the flow characteristics.

Mathematical formulation

The analysis involves an incompressible laminar flow of a viscous fluid between two horizontal parallel Riga plates. The lower plate remains stationary at $\tilde{y}=0$ while the upper plate, located at a distance $\tilde{y}=d$, moves with a constant velocity U_0, denoted by $\pi\upsilon/l$. In the assumed configuration, the flow direction is aligned with the $\tilde{x}$-axis, the $\tilde{y}$-axis is perpendicular to the flow, and the width of the plates runs parallel to the $\tilde{x}\tilde{z}$-plane. The two plates remain stationary at consistent temperatures. Assuming T_1 as the temperature of the lower plate and T_2 for the upper plate, where $T_2 > T_1$. The fluid's initial temperature is considered to be identical to the temperature of the lower plate T_1. As the plates extend infinitely in the $\tilde{x}$- and $\tilde{z}$-directions, physical variables, except for pressure, remain constant along these dimensions. *i.e.* $\frac{\partial A}{\partial \tilde{x}} = \frac{\partial A}{\partial \tilde{z}} = 0$, where $A \rightarrow$ physical variables except pressure. In the context of a generalized Couette flow, the applied pressure gradient $\frac{\partial \tilde{p}}{\partial \tilde{x}} = (\mathrm{P})$ on the fluid remains consistently constant. The schematic representation of the problem's physical model is illustrated in *Figure 1*.

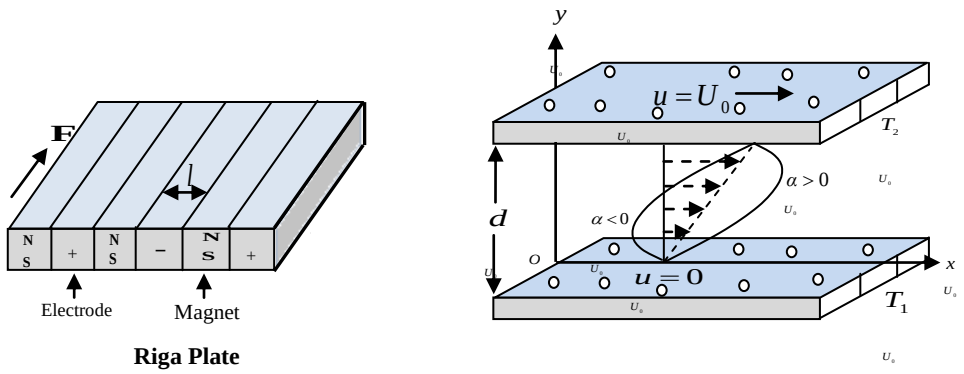

Figure 1. *Physical model of the system.*

Certainly, in the context of the Riga plate, a uniform magnetic force is generated, and the Lorentz force is defined as the magnetic force. The Lorentz force arises from the interaction between the magnetic field and the electric current in the presence of charged particles, as described by the Lorentz force equation $\bar{f} = \mathbf{J} \wedge \mathbf{B} \approx \sigma(\mathbf{E} \wedge \mathbf{B})$. In the case of the Riga plate, the Lorentz force would be associated with the interaction between the magnetic field generated by the plate and any charged particles or currents

in the surrounding medium. As per the Grinberg hypothesis, these magnetic forces can be defined in the following (Eq. 1):

$$\text{manner } \bar{f} = \mathbf{J} \wedge \mathbf{B} = \left(\frac{\pi}{8} J_0 M_0 e^{-\frac{\pi}{l} y} \ , \ 0 \ , \ \frac{\pi}{8} J_0 M_0 e^{-\frac{\pi}{l} y} \right) \quad \text{Eq. (1)}$$

Assuming Couette flow and employing Bousniques approximations, the dimensional expressions for the momentum and energy equations are established as follows (Eq. 2 to Eq. 4):

$$\frac{\partial \tilde{u}}{\partial \tilde{t}} - v_0 \frac{\partial \tilde{u}}{\partial \tilde{y}} = -\frac{\mathrm{P}}{\rho} + \upsilon \frac{\partial^2 \tilde{u}}{\partial \tilde{y}^2} + \frac{\pi}{8\rho} J_0 M_0 e^{-\frac{\pi}{a} \tilde{y}} \quad \text{Eq. (2)}$$

$$\frac{\partial \tilde{w}}{\partial \tilde{t}} - v_0 \frac{\partial \tilde{w}}{\partial \tilde{y}} = \upsilon \frac{\partial^2 \tilde{w}}{\partial \tilde{y}^2} + \frac{\pi}{8\rho} J_0 M_0 e^{-\frac{\pi}{a} \tilde{y}} \quad \text{Eq. (3)}$$

$$\frac{\partial \tilde{T}}{\partial \tilde{t}} - v_0 \frac{\partial \tilde{T}}{\partial \tilde{y}} = \frac{k}{\rho C_p} \frac{\partial^2 \tilde{T}}{\partial \tilde{y}^2} + \frac{\mu}{\rho c_p} \left(\frac{\partial \tilde{w}}{\partial \tilde{y}} \right)^2 \quad \text{Eq. (4)}$$

The associated boundary conditions are (Eq. 5)

$$t \le 0 : \quad u = 0, \quad w =, \ T = T_1 \text{ for all } y \ge 0$$

$$t > 0 : \begin{cases} u = 0, \quad w = 0, \ T = T_1 \text{ at } \ y = 0 \\ u = \dfrac{\pi \upsilon}{l}, \ w = 0, \ T = T_2 \quad \text{at } \ y = d \end{cases} \quad \text{Eq. (5)}$$

To obtain the non-dimensional representation of the aforementioned equations, introduce the subsequent non-dimensional variables (Eq. 6):

$$x = \frac{\pi}{l} \tilde{x}, \quad y = \frac{\pi}{l} \tilde{y}, \qquad u = \frac{l}{\pi \upsilon} \tilde{u}, \qquad w = \frac{l}{\pi \upsilon} \tilde{w}, \qquad t = \frac{\pi^2 \upsilon}{l^2} \tilde{t}, \qquad \theta = \frac{\tilde{T} - \tilde{T}_1}{\tilde{T}_2 - \tilde{T}_1} \quad \text{Eq. (6)}$$

Through the utilization of these dimensionless variables in the aforementioned equations, the resulting non-dimensionalized form of the governing equations has been determined (Eq. 7 to Eq. 9).

$$\frac{\partial u}{\partial t} - V_0 \frac{\partial u}{\partial y} = \alpha + \frac{\partial^2 u}{\partial y^2} + H_r e^{-y} \quad \text{Eq. (7)}$$

$$\frac{\partial w}{\partial t} - V_0 \frac{\partial w}{\partial y} = \frac{\partial^2 w}{\partial y^2} + H_r e^{-y} \quad \text{Eq. (8)}$$

$$\frac{\partial \theta}{\partial t} - V_0 \frac{\partial \theta}{\partial y} = \frac{1}{P_r} \frac{\partial^2 \theta}{\partial y^2} - E_c \left(\frac{\partial w}{\partial y} \right)^2 \quad \text{Eq. (9)}$$

The corresponding boundary conditions are (Eq. 10):

$$t \le 0: \quad u = 0,\ \theta = 0, \quad \text{for all } y \ge 0$$
$$t > 0: \begin{cases} u = 0, & w = 0, \quad \theta = 0 \ \text{ at } \ y = 0 \\ u = 1, & w = 0, \ \theta \to 1, \ \text{at } \ y \to d \end{cases} \qquad \text{Eq. (10)}$$

Where $\alpha = -\frac{l^3 \mathrm{P}}{\rho \upsilon^2 \pi^3}$ = Dimensionless pressure gradient; $H_r = \frac{l^3 J_0 M_0}{8 \rho \upsilon^2 \pi^2} =$ Modified Hartmann Number; $P_r = \frac{\rho c_p \upsilon}{k}$ the Prandtl number and $E_c = \frac{\upsilon^2 \pi^2}{(\tilde{T}_2 - \tilde{T}_1) c_p l^2}$ is the Eckert Number.

Materials and Methods

The set of non-dimensional coupled partial differential equations (5)-(7) was addressed through explicit finite difference methods, taking into account the corresponding boundary conditions (8).It is considered maximum length of the plate is $x_{\max}(=10)$ and distance between the plates $d = 2$ *i.e.* $y_{\max} = 2$ as the lower plate is fixed at $y = 0$. This means x varies from 0 to 10 and y varies from 0 to 2. The finite difference schemes employed for addressing the given problems are outlined as follows (Eq. 11 to Eq. 14):

$$\frac{u_{i,j}^{k+1} - u_{i,j}^{k}}{\Delta t} - V_0 \frac{u_{i,j}^{k} - u_{i,j-1}^{k}}{\Delta y} = \alpha + \frac{u_{i,j+1}^{k} - 2u_{i,j}^{k} + u_{i,j-1}^{k}}{\Delta y^2} + H_r e^{-y_i} \qquad \text{Eq. (11)}$$

$$\frac{w_{i,j}^{k+1} - w_{i,j}^{k}}{\Delta t} - V_0 \frac{w_{i,j}^{k} - w_{i,j-1}^{k}}{l} = \frac{w_{i,j+1}^{k} - 2w_{i,j}^{k} + w_{i,j-1}^{k}}{l^2} + H_r e^{-y_i} \qquad \text{Eq. (12)}$$

$$\frac{\theta_{i,j}^{k+1} - \theta_{i,j}^{k}}{\Delta t} - V_0 \frac{\theta_{i,j}^{k} - \theta_{i,j-1}^{k}}{\Delta y} = \frac{1}{P_r} \left(\frac{\theta_{i,j+1}^{k} - 2\theta_{i,j}^{k} + \theta_{i,j-1}^{k}}{\Delta y^2} \right) - E_c \frac{w_{i,j}^{k} - w_{i,j-1}^{k}}{\Delta y} \qquad \text{Eq. (13)}$$

with the boundary conditions:

$$t \le 0: \quad u_{i,j}^{k} = 0,\ \theta_{i,j}^{k} = 0, \quad \text{for all } y \ge 0$$
$$t > 0: \begin{cases} u_{i,j}^{k} = 0, & w_{i,j}^{k} = 0, \quad \theta_{i,j}^{k} = 0 \ \text{ at } \ y = 0 \\ u_{i,j}^{k} = 1, & w_{i,j}^{k} = 0, \ \theta_{i,j}^{k} = 1, \ \text{at } \ y = d \end{cases} \qquad \text{Eq. (14)}$$

Here, the subscripts *i* and *j* refer to *x* and *y* and the superscript *k* refers to time *t*.

Shear stresses and Nusselt number

The examination delved into the influence of pertinent factors on the shear stress derived from fluid velocity, considering both local and average values. The expressions for non-dimensional local and average shear stress in the fluid are indicated by the relationships designated as $\tau_L = \mu \left. \frac{\partial u}{\partial y} \right|_{y=0}$ and $\tau_A = \frac{1}{L} \int_0^L \mu \left. \frac{\partial u}{\partial y} \right|_{y=0} dx$ respectively. The Nusselt number is characterized as the rate of heat transfer at the plate. The expressions

for the local and average Nusselt number in the fluid are provided by $Nu_L = -\mu \frac{\partial \theta}{\partial y}\Big|_{y=0}$ and $Nu_A = -\frac{1}{L}\int_0^L \mu \frac{\partial \theta}{\partial y}\Big|_{y=0} dx$.

Results and Discussion

The numerical findings and graphical representations of fluid velocity and temperature distributions are elucidated, considering the influence of pertinent non-dimensional parameters, including the Pressure gradient parameter (α), modified Hartmann number (H_r), Suction velocity parameter (V_0), Prandtl number (P_r), and Eckert number (E_c). The investigation examines the effects of these parameters on the required profiles while keeping the values of $\alpha = 2.0$, $H_r = 1.0$, $V_0 = 2.0$, $P_r = 0.71$, and $E_c = 0.5$. It is noted that *u* is referred to as primary velocity and *w* referred to as secondary velocity.

Mesh and time sensitivity test

Graphical illustrations have been utilized to elaborate on the influence of different parameters on the velocity and temperature profiles. *Figures 2(a)* to *Figure 2(c)* illustrate the fluid velocities and temperature distributions *u*, *w* and θ at various time instances τ. The computations were performed for various time instances, as $\tau = 1, 3, 6$ and 8 utilizing a specified time step size $\Delta t = 0.0005$. It is evident from the figures that there is no discernible change after $\tau = 8$ for *u*, *w* and θ. *Figures 3(a)* to *Figure 3(c)* demonstrate the effectiveness of the grid pairs in capturing the primary and secondary velocities *u*, *w* and the temperature θ. It has displayed the velocity and temperature distributions for three sets of grids $n = 40$, $n = 45$ and $n = 50$ considering time $\tau = 8$ and time step $\Delta t = 0.0005$. Moreover, minimal variation is noted among these grid pairs, suggesting that any of them is considered acceptable for determining the steady-state solution. The same observation is valid for the other distributions. The steady-state solution has been attained within a time of at least $\tau > 7$. In this ongoing analysis, the following graphs have been generated using the chosen time $\tau = 8$, grid spacing $n = 40$, and time step $\Delta t = 0.0005$.

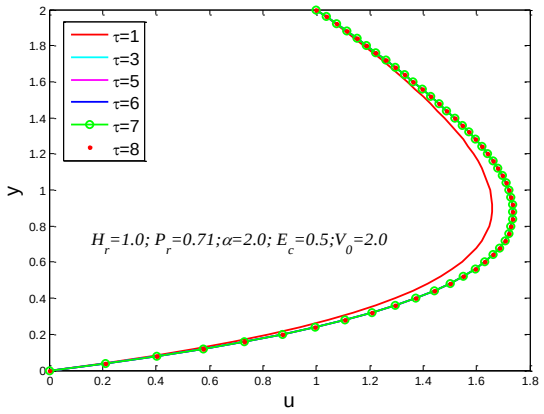

Figure 2(a). *Time sensitivity on primary velocity u.*

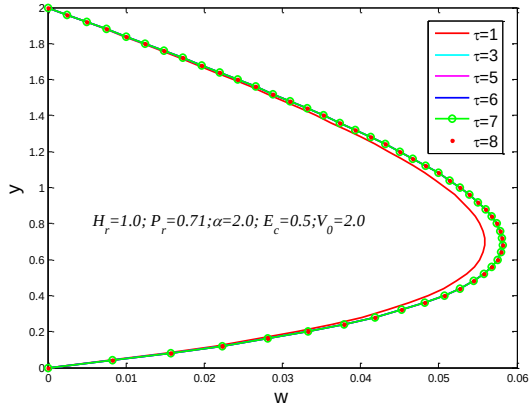

Figure 2(b). *Time sensitivity on secondary velocity w.*

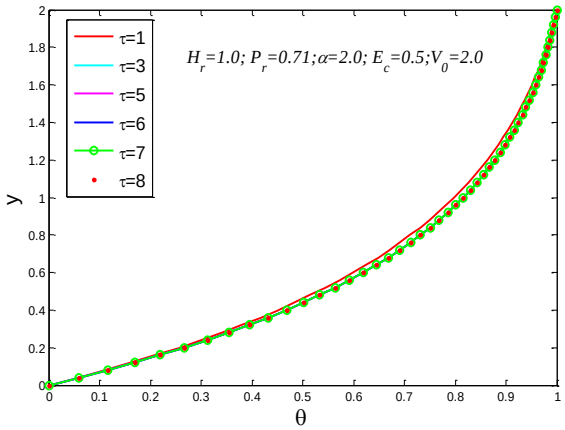

Figure 2(c). *Time sensitivity on temperature* θ.

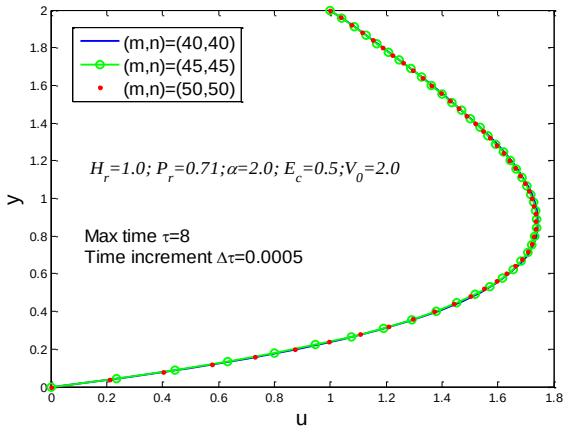

Figure 3(a). *Mesh sensitivity on primary velocity u.*

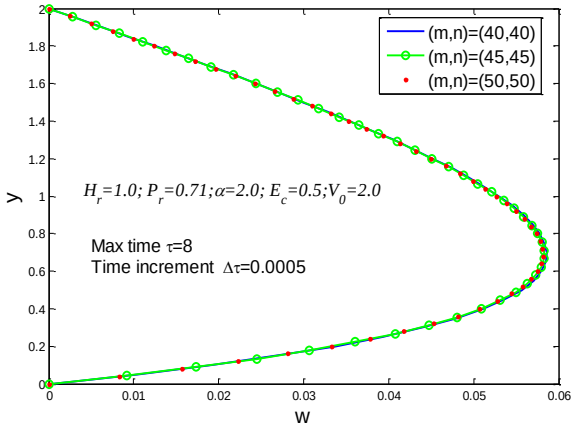

Figure 3(b). *Mesh sensitivity on secondary velocity w.*

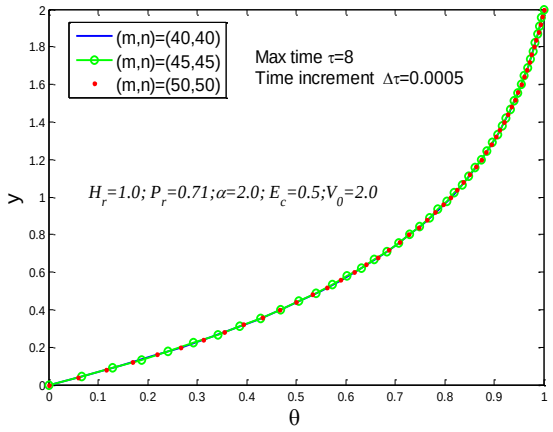

Figure 3(c). *Mesh sensitivity on temperature* θ.

Effects of various parameters

To analyze the physical aspects of the problem, *Figure 4* to *Figure 6* present the distributions of primary velocity, local shear stress, and average shear stress along the *x*-direction, respectively. *Figure 4(a)* to *Figure 4(c)* demonstrate the impact of dimensionless pressure gradient (α) on the primary velocity. Since $\alpha = -l^3 \mathrm{P}/(\rho \upsilon^2 \pi^3)$, it means that $\alpha > 0$ where a constant pressure gradient (P) diminishes in the direction of motion, the primary velocity *u* exhibits an increasing trend with the rise of α across the entire width between the plates. However, the influence of $\alpha < 0$ indicates that pressure gradient (P) increases in the direction of motion, leading to a reversal in the primary velocity *u* as illustrated in *Figure 4(a)*. A consistent pattern is observed for both local and average shear stress on the fluid, as depicted in *Figure 4(a)* to *Figure 4(c)*, respectively. The effects of the modified Hartmann number on the primary velocity (u), local (τ_{xL}) and the average shear stress (τ_{xA}) are shown in the *Figure 5(a)* to *Figure 5(c)*, respectively. The changed modified Hartmann number causes an increase in skin friction. Due to the Riga plate Lorentz force plays an opposing role to flow for $H_r < 0$. It is clear that under the influence of H_r, the primary velocity, local shear stress, and average shear stress are all having a decreasing impact due to the Riga plate. The

Lorentz force plays both a helpful and an opposing role in the fluid's velocity, which reduces as H_r decreases. *Figure 6(a)* to *Figure 6(c)* depict the impact of the suction velocity parameter (V_0) on the primary velocity (u) as well as the characteristics of local shear stress (τ_{xL}) and average shear stress (τ_{xA}). The observation indicates that the primary velocity (u) exhibits a cross flow. The demonstrated trend reveals an increasing effect within the interval $0 < y < 0.56$ after that it has a decreasing effect and local shear stress (τ_{xL}) and average shear stress (τ_{xA}) are increase with the increasing values of Suction velocity parameter (V_0).

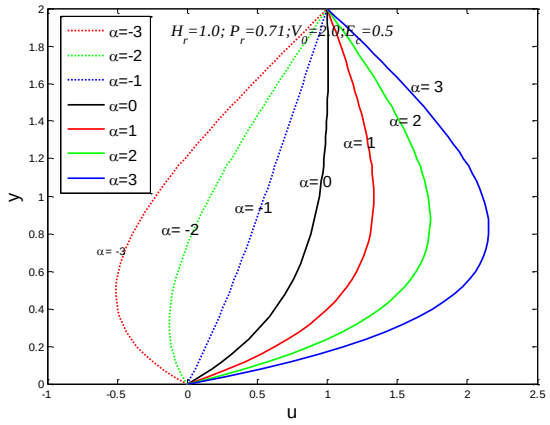

Figure 4(a). *Effect of a pressure gradient parameter on primary velocity.*

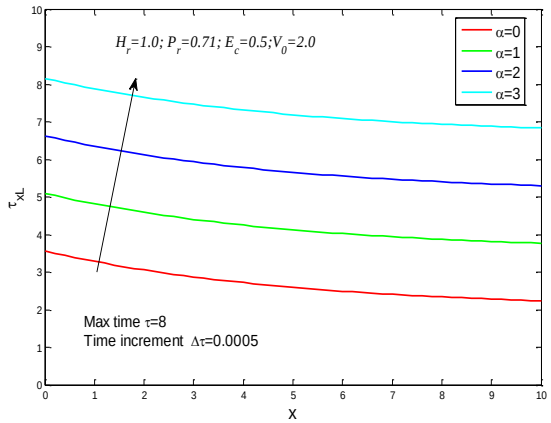

Figure 4(b). *Effect of a pressure gradient parameter on local shear stress.*

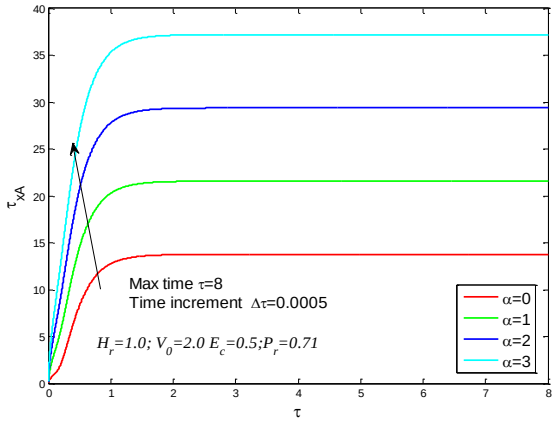

Figure 4(c). *Effect of a pressure gradient parameter on average shear stress.*

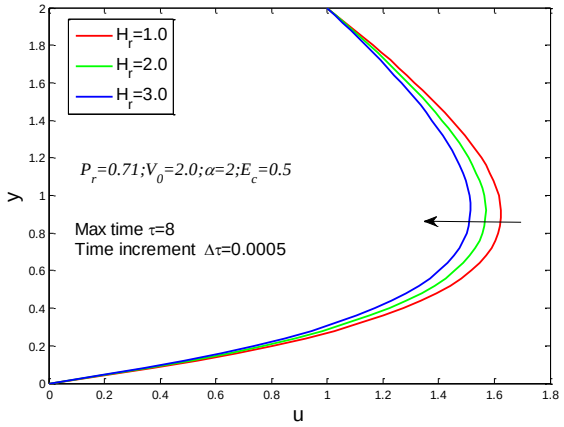

Figure 5(a). *Effect of modified Hartmann number on primary velocity.*

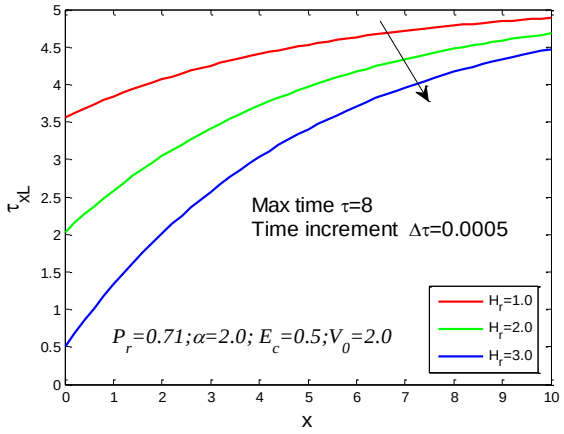

Figure 5(b). *Effect of modified Hartmann number on local shear stress.*

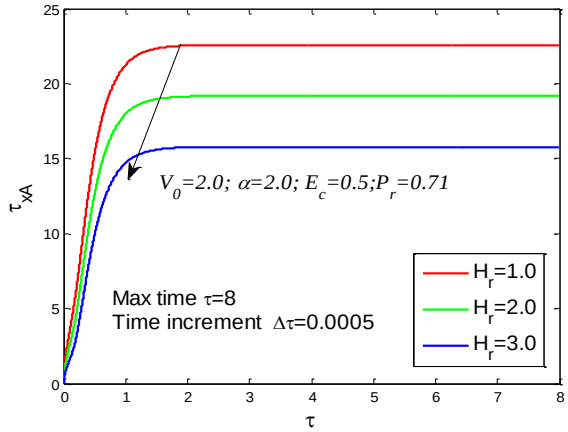

Figure 5(c). *Effect of modified Hartmann number on average shear stress.*

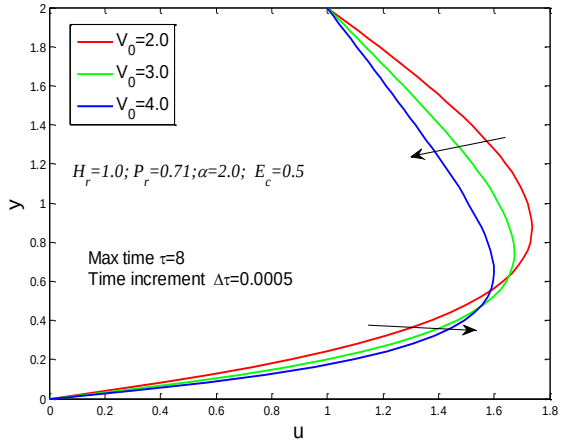

Figure 6(a). *Effect of suction velocity parameter on primary velocity.*

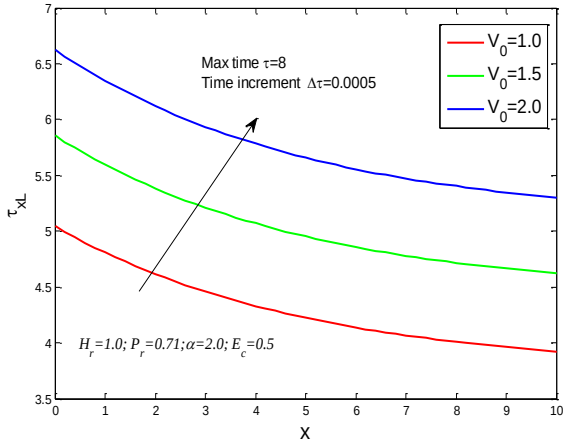

Figure 6(b). *Effect of suction velocity parameter on local shear stress.*

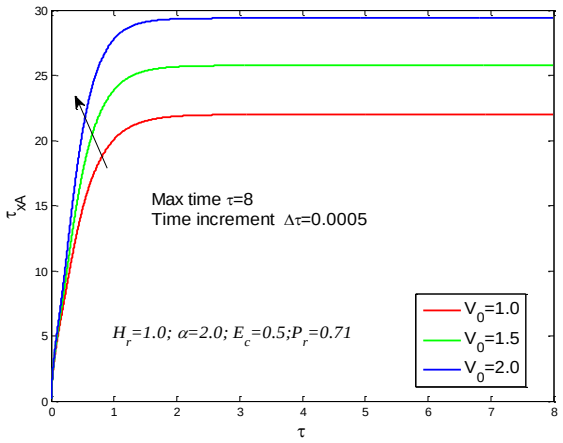

Figure 6(c). *Effect of suction velocity parameter on average shear stress.*

Figure 7 to *Figure 8* illustrate the distribution of secondary velocity *(w)*, local shear stress (τ_{zL}), and average shear stress (τ_{zA}) along the *y*-direction, respectively. The secondary velocity *(w)* profile is plotted for the modified Hartman number (H_r), local (τ_{zL}) and the average shear stress (τ_{zA}) are depicted in *Figure 7(a)* to *Figure 7(c)*. The Lorentz force plays both a helpful and an opposing role in the fluid's velocity *(w)*, due to the Riga plate which reduces as H_r decreases. Here with the increasing values of H_r it has found the decreasing effect of local shear stress (τ_{zL}), and average shear stress (τ_{zA}). *Figure 8(a)* to *Figure 8(c)* are created to clarify the influence of the suction parameter on velocity (V_0), local shear stress (τ_{zL}), and average shear stress (τ_{zA}), respectively. It signifies the rising impact of suction velocity, the declining effect of secondary velocity *(w)*, and both local shear stress (τ_{zL}) and average shear stress (τ_{zA}) display an increasing effect.

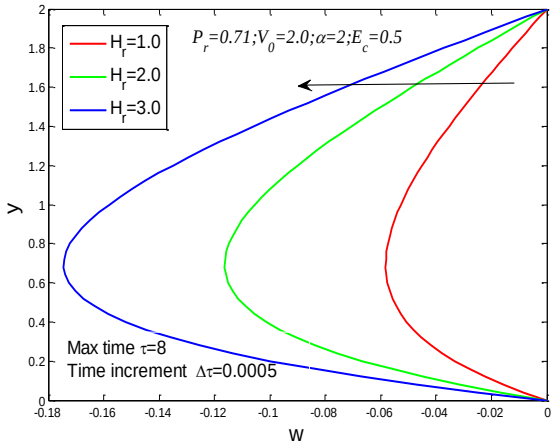

Figure 7(a). *Effect of the modified Hartman member on secondary velocity.*

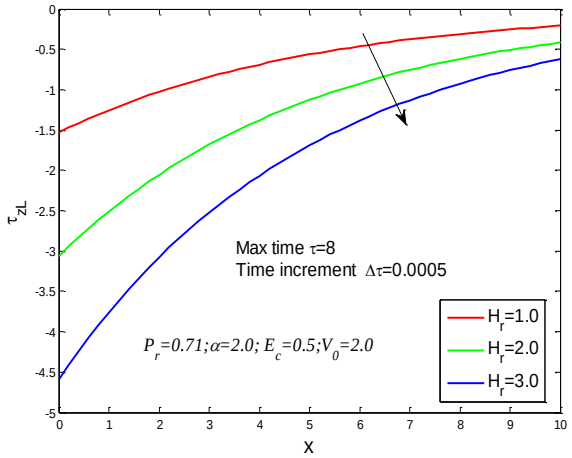

Figure 7(b). *Effect of the modified Hartman number on local shear stress.*

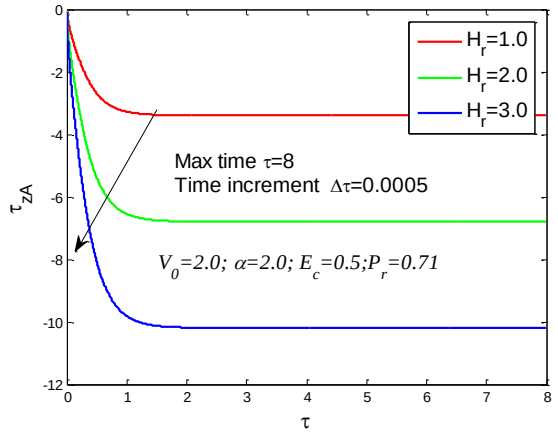

Figure 7(c). *Effect of the modified Hartman number on average shear stress.*

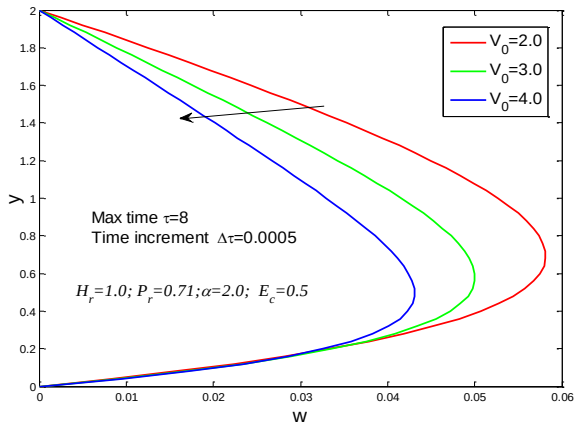

Figure 8(a). *Effect of suction velocity parameter on the secondary velocity.*

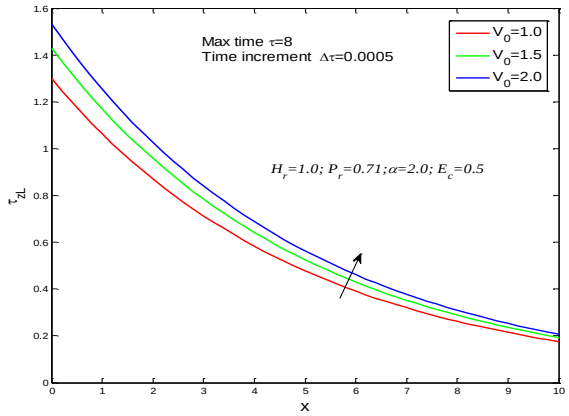

Figure 8(b). *Effect of suction velocity parameter on local shear stress.*

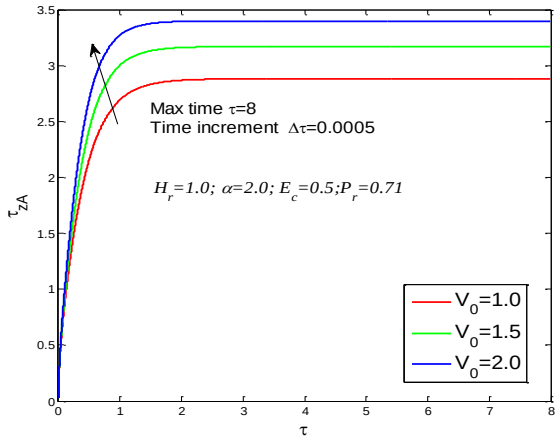

Figure 8(c). *Effect of suction velocity parameter on average shear stress.*

Figure 9 to *Figure 12* illustrate the distribution of temperature, local Nusselt number, and average Nusselt number, respectively. The *Figure 9(a)* to *Figure 9(c)* illustrate that with an increase in the modified Hartman number (H_r), there is a notable decrease in temperature (θ), as well as in both the Nusselt number and average Nusselt number. The impacts of the suction parameter on temperature, local Nusselt number, and average Nusselt number are depicted in *Figure 10(a)* to *Figure 10(c)* respectively. The impacts of the Suction parameter (V_0) on temperature (θ), local Nusselt number (Nu_L), and average Nusselt number (Nu_A) are depicted in *Figure 10(a)* to *Figure 10(c)* respectively. The temperature profile (θ)experiences an increase due to the rising impact of the Prandtl number(P_r), as observed in *Figure 11(a)*. In contrast, *Figure 11(b)* and *Figure 11(c)* demonstrate the opposite effect of (θ). *Figure 12(a)* to *Figure 12(c)* depict the influence of the Eckert number (E_c) on the temperature (θ), local Nusselt number (Nu_L), and average Nusselt number (Nu_A), respectively. It is observed from *Figure 12(a)* to *Figure 12(c)* the effects of Eckert number (E_c) on the temperature (θ)local Nusselt number (Nu_L) and on the average Nusselt number (Nu_A) respectively. The displayed results indicate that the temperature profile exhibits an increasing trend, and both local and average Nusselt numbers also demonstrate an increasing effect.

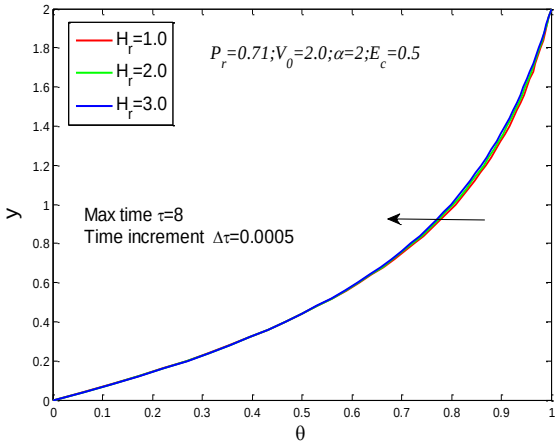

Figure 9(a). *Effect of modified Hartman number on temperature.*

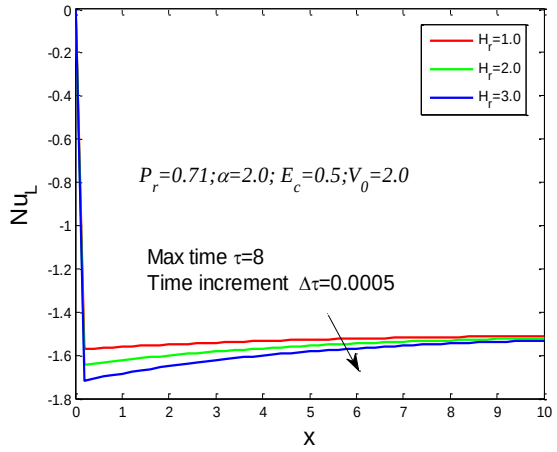

Figure 9(b). *Effect of modified Hartman number on Nusselt number.*

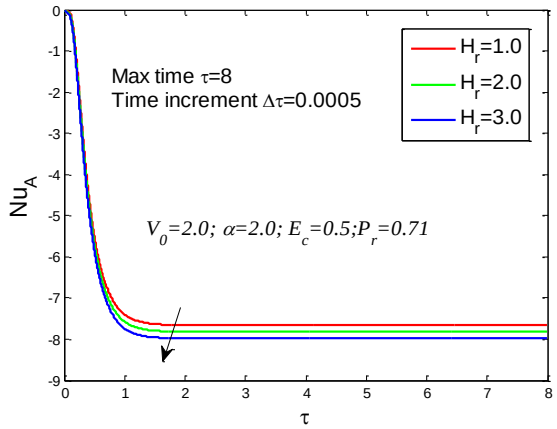

Figure 9(c). *Effect of modified Hartman number on average Nusselt number.*

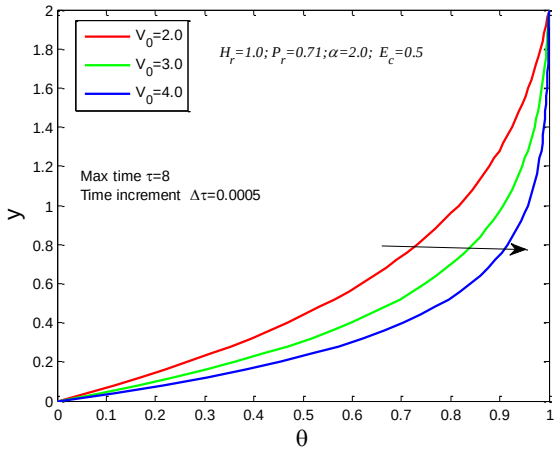

Figure 10(a). *Effect of suction velocity parameter on temperature.*

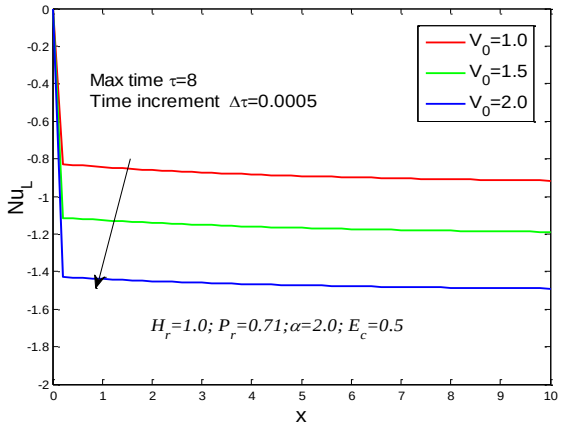

Figure 10(b). *Effect of suction velocity parameter on local Nusselt number.*

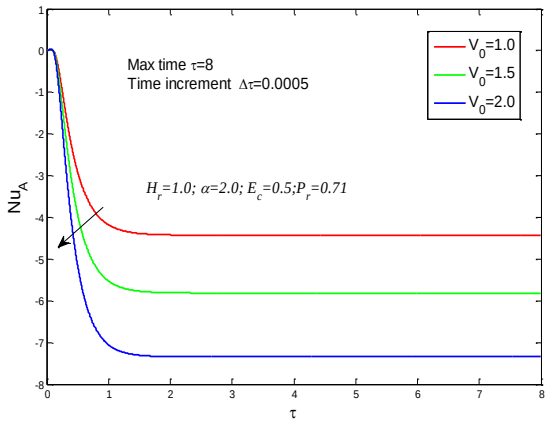

Figure 10(c). *Effect of suction velocity parameter on average Nusselt number.*

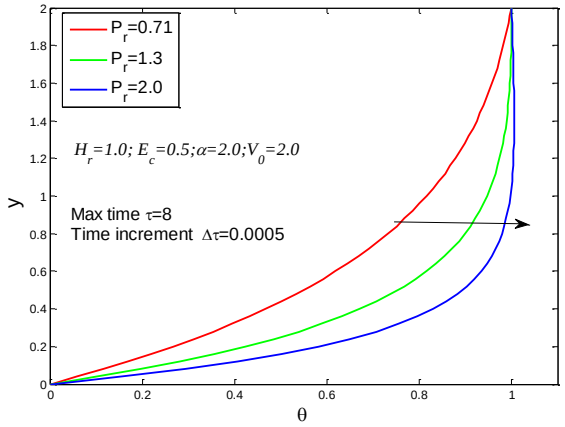

Figure 11(a). *Effect of Prandtl number on temperature.*

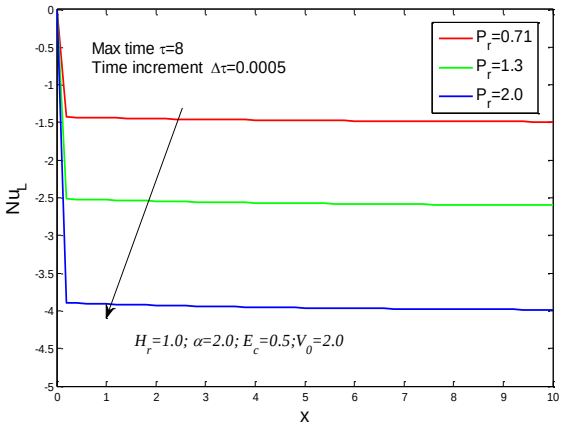

Figure 11(b). *Effect of Prandtl number on local Nusselt number.*

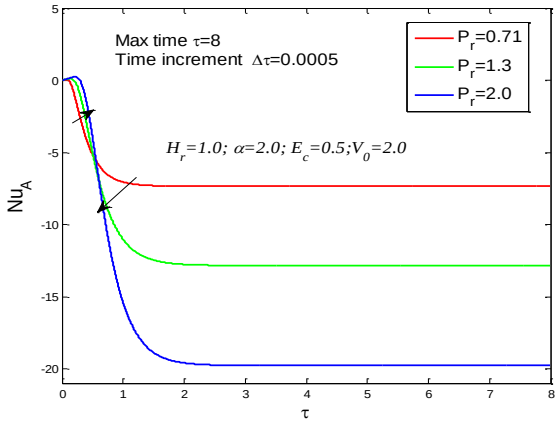

Figure 11(c). *Effect of Prandtl number on average Nusselt number.*

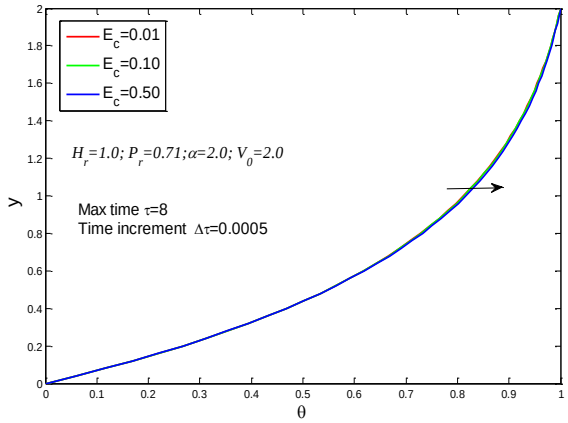

Figure 12(a). *Effect of Eckert number on temperature.*

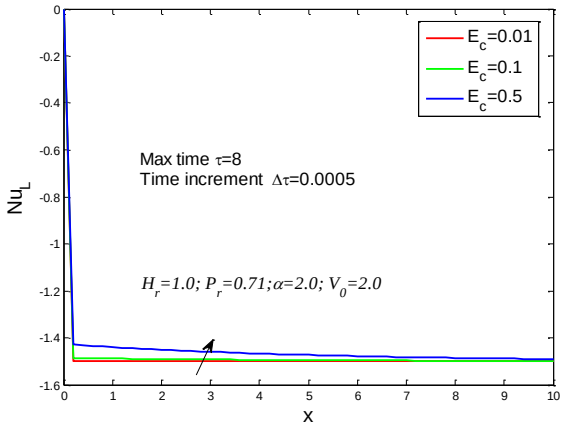

Figure 12(b). *Effect of Eckert number on local Nusselt number.*

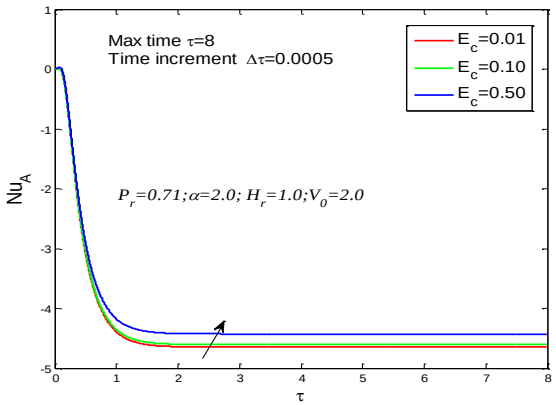

Figure 12(c). *Effect of Eckert number on average Nusselt number.*

Validation test and general discussion

To show the validity of our numerical simulation it is compared with the previously published result and its graphical results executed by MATLAB code, which are shown in *Figure 13*. In this study, the numerical model of Couette fluid flows across a parallel Riga plate has been created with an electromagnetic field. Various aspects of flow

characteristics are examined concerning the influence of relevant non-dimensional parameters, specifically the pressure gradient parameter (α), modified Hartmann number (H_r), suction velocity parameter (V_0), Prandtl number (P_r), and Eckert number (E_c). The effects of those parameters on the necessary profiles are investigated with the fixed values of $\alpha = 2.0$, $H_r = 1.0$, $V_0 = 2.0$, $P_r = 0.71$, and $E_c = 0.5$. The finite difference method served as the primary tool for obtaining a steady solution. It is observed that the current study is expanded to include more investigation into Couette fluid flows in light of the analysis approach and the trends of the data. A comparison of our results with the published results for the Couette flow has been discussed clearly. In this case, the comparisons have been performed by the Book-Boundary Layer Theory by H. Schlichting and our numerical results. As can be seen, the velocity profile of the Couette flow had the same pattern as the Book-Fluid dynamics by H. Schlichting.

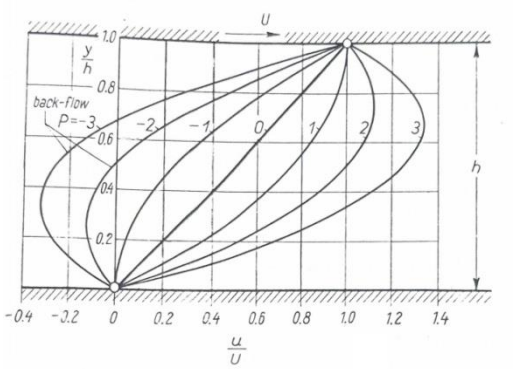

Figure 13(a). *Effect of Pressure gradient Parameter on velocity distribution results (Book-Fluid dynamics by H. Schlichting)*

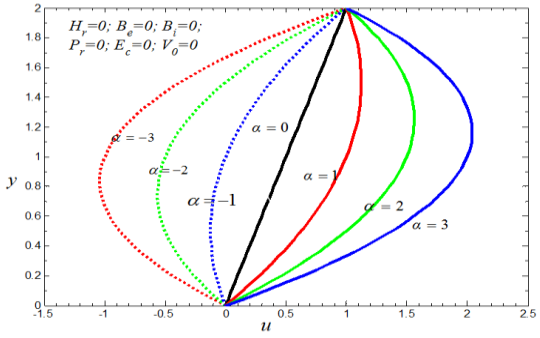

Figure 13(b). *Effect of Pressure gradient Parameter on velocity distribution by current numerical result.*

Conclusion

Overall, both qualitatively and numerically, the comparisons presented are in good agreement with the findings of the experiment. It's also fascinating to contrast the outcomes of the experimental research with those of the current investigation. The results of our recent studies are briefly presented for the impact of pertinent non-dimensional parameters namely Pressure gradient parameter (α), modified Hartmann number (H_r), Suction velocity parameter (V_0), Prandtl number (P_r) and Eckert

number(E_c).The experimental results have been thoroughly and accurately compared to the current numerical results. Consequently, there is a possibility that the findings of the study are valid. Summarizing the outcomes, which are derived from the comprehensive investigation of the relevant parameters mentioned above. (1) The primary velocity profile (*u)* shows an increase with higher values of the Pressure gradient parameter(α), but it experiences a decrease as the modified Hartmann number(H_r) increases. The Suction parameter (V_0) exhibits a cross effect, leading to an elevation in skin friction with an increase in the suction parameter. (2) Secondary velocity profile (*w)* decreases for increasing values of the modified Hartmann number(H_r). For the rising values of Suction parameter(V_0) the secondary velocity profile (*w)* decreases where the skin friction coefficient is increased. (3) The temperature profile decreases with the rising values of the modified Hartmann number(H_r). For the increasing values of theV_0, P_r andE_c the temperature profile increases where the local and average Nusselt numbers show the reverse effects for V_0 andP_r.

Acknowledgement

The research study is self-funded.

Conflict of interest

The authors declare that there is no conflict of interest involve in this research study.

REFERENCES

[1] Ahmad, A., Asghar, S., Afzal, S. (2016): Flow of nanofluid past a Riga plate. – Journal of Magnetism and Magnetic Materials 402: 44-48.
[2] Al-Nimr, M.A., Masoud, S. (1998): Unsteady free convection flow over a vertical flat plate immersed in a porous medium. – Fluid Dynamics Research 23(3): 153-160.
[3] Angirasa, D., Peterson, G.P. (1997): Natural convection heat transfer from an isothermal vertical surface to a fluid saturated thermally stratified porous medium. – International Journal of Heat and Mass Transfer 40(18): 4329-4335.
[4] Attia, H.A., Ewis, K.M. (2010): Unsteady MHD Couette flow with heat transfer of a viscoelastic fluid under exponential decaying pressure gradient. – Journal of Applied Science and Engineering 13(4): 359-364.
[5] Ayub, M., Abbas, T., Bhatti, M.M. (2016): Inspiration of slip effects on electromagnetohydrodynamics (EMHD) nanofluid flow through a horizontal Riga plate. – The European Physical Journal Plus 131(6): 1-9.
[6] Bég, O.A., Zueco, J., Takhar, H.S. (2009): Unsteady magnetohydrodynamic Hartmann–Couette flow and heat transfer in a Darcian channel with Hall current, ionslip, viscous and Joule heating effects: Network numerical solutions. – Communications in Nonlinear Science and Numerical Simulation 14(4): 1082-1097.
[7] Chauhan, D.S., Rastogi, P. (2009): Hall current and heat transfer effects on MHD flow in a channel partially filled with a porous medium in a rotating system. – Turkish Journal of Engineering and Environmental Sciences 33(3): 167-184.
[8] Das, S., Maji, S.L., Guria, M., Jana, R.N. (2009): Unsteady MHD Couette flow in a rotating system. – Mathematical and Computer Modelling 50(7-8): 1211-1217.

[9] Fang, T. (2004): A note on the incompressible Couette flow with porous walls. – International Communications in Heat and Mass Transfer 31(1): 31-41.
[10] Gailitis, A. (1961): On a possibility to reduce the hydrodynamical resistance of a plate in an electrolyte. – Applied Magnetohydrodynmics 12: 143-146.
[11] Hasimoto, H. (1957): Boundary layer growth on a flat plate with suction or injection. – Journal of the Physical Society of Japan 12(1): 68-72.
[12] Kuznetsov, A.V. (1998): Analytical investigation of Couette flow in a composite channel partially filled with a porous medium and partially with a clear fluid. – International Journal of Heat and Mass Transfer 41(16): 2556-2560.
[13] Muhuri, K.P. (1963): Flow formation in Couette motion in magnetohydrodynamics with suction. – Journal of the Physical Society of Japan 18(11): 1671-1675.
[14] Ochoa-Tapia, J.A., Whitaker, S. (1995a): Momentum transfer at the boundary between a porous medium and a homogeneous fluid-I. – Theoretical development. International Journal of Heat and Mass Transfer 38(14): 2635-2646.
[15] Ochoa-Tapia, J.A., Whitaker, S. (1995b): Momentum transfer at the boundary between a porous medium and a homogeneous fluid-II. – Comparison with experiment. International Journal of Heat and Mass Transfer 38(14): 2647-2655.
[16] Pantokratoras, A. (2011): The Blasius and Sakiadis flow along a Riga-plate. – Progress in Computational Fluid Dynamics, An International Journal 11(5): 329-333.
[17] Pantokratoras, A., Magyari, E. (2009): EMHD free-convection boundary-layer flow from a Riga-plate. – Journal of Engineering Mathematics 64(3): 303-315.
[18] Raptis, A., Kafousias, N. (1982): Magnetohydrodynamic free convective flow and mass transfer through a porous medium bounded by an infinite vertical porous plate with constant heat flux. – Canadian Journal of Physics 60(12): 1725-1729.
[19] Ravikumar, V., Raju, M.C., Raju, G.S.S. (2012): MHD three dimensional Couette flow past a porous plate with heat transfer. – IOSR Jour. Maths. 1(3): 3-9.
[20] Sacheti, N.C., Chandran, P., Singh, A.K. (1994): An exact solution for unsteady magnetohydrodynamic free convection flow with constant heat flux. – International Communications in Heat and Mass Transfer 21(1): 131-142.
[21] Seth, G.S., Ansari, M.S., Nandkeolyar, R. (2011): Unsteady hydromagnetic couette flow within a porous channel. – Journal of Applied Science and Engineering 14(1): 7-14.
[22] Soundalgekar, V.M., Gupta, S.K., Birajdar, N.S. (1979): Effects of mass transfer and free convection currents on MHD Stokes' problem for a vertical plate. – Nuclear Engineering and Design 53(3): 339-346.
[23] Yabo, I.B., Jha, B.K., Lin, J.E. (2018): On a Couette flow of conducting fluid. – International Journal of Theoretical and Applied Mathematics 4(1): 8-21.